Investigations of the effect of electrode gap on the performance of a corona charger having separated corona and charging zones

Q1 M. Domat [a,*], F.E. Kruis [b], J.M. Fernandez-Diaz [a]

[a] Department of Physics, University of Oviedo, C/Calvo Sotelo, s/n, E-33007 Oviedo, Spain
[b] Institute for Nanostructures and Technology (NST) and Center for Nanointegration Duisburg-Essen (CENIDE), University of Duisburg-Essen, Bismarckstr. 81, D-47057 Duisburg, Germany

ARTICLE INFO

ABSTRACT

An efficient and a versatile unipolar corona charger was developed. It has indirect charging characteristics, with corona and charging regions separated. Ions were generated by a needle electrode and then driven to the charging region by a sheath flow in order to reduce the electrostatic loss of nanoparticles. The distance of the electrode to the walls can be adjusted by a micrometer, modifying the onset voltage and $N_i t$–product, and therefore the intrinsic and extrinsic charging efficiencies and loss of charged particles. Experimental results indicate that the generated ion current is practically the same independent of the variation in the applied voltage or corona current, but varying the electrode gap distance seems to be a much more efficient way to regulate the $N_i t$–product. The charging efficiency can vary from high values, comparable to the higher efficiency chargers presented in the literature, to lower levels such as reached with bipolar chargers.

© 2013 Published by Elsevier Ltd.

1. Introduction

Providing electrical charge to particles is a fundamental requirement for particle characterization by mobility analysis. The calculation of the aerosol size distribution requires an accurate knowledge of the charge level and charge distribution of the incoming aerosol. Although bipolar radioactive chargers are the most widely used devices due to their well-defined charge distribution, unipolar diffusion chargers are still at the focus of interest, due to their simplicity.

Q3 Corona chargers have been studied for a long time (Alguacil & Alonso, 2006; Biskos et al., 2005a; Büscher et al., 1994; Hewitt, 1957; Intra & Tippayawong, 2010; Kruis & Fissan, 2001; Liu & Pui, 1975; Medved et al., 2000). They can attain higher charging levels than radioactive chargers so that a lower concentration threshold can be reached with electrometers. Due to the absence of ion recombination, unipolar ionization results in higher ion concentrations than bipolar ionization. Furthermore, they are exempt from expensive safety precautions and severe legal restrictions caused by the use of the radioactive sources.

However, some difficulties have to be overcome before designing a new prototype. Reported problems are related with the following issues (Kim et al., 2010; Kwon et al., 2006):

1. *Ozone production*: During an electrostatic discharge in a gas such as air (78% N_2, 21% O_2 approx.), some diatomic oxygen molecules from air are split and recombine to form ozone, which is unstable, toxic and a strong oxidant for metals.

Q2 * Corresponding author. Tel.: +34 659390180.
E-mail address: maida.dro@gmail.com (M. Domat).

As a result, the discharge electrode can be altered and therefore the charging conditions of the corona device. For this reason, a gas different from air is preferably used when possible.

2. *Nanoparticle generation*: One of the advantages of the radioactive neutralizers over the corona discharge is the stability of the first ones. In corona devices the usage of the electrode can wear it out and change its geometry, leading to a change in charging efficiency levels. It could also promote the formation of new particles, either from erosion and sputtering from the electrode itself or from gaseous contaminants present in the gas (Alonso et al., 2006; Kleefsman & Van Gulijk, 2008).

3. *AC or DC electric field*: Although the previously presented corona devices used either direct or alternate current, it has been recently reported that the AC field offers no benefit compared to the DC field (Marquard et al., 2006a). Comparing the devices with AC (Biskos et al., 2005b; Büscher et al., 1994; Kruis & Fissan, 2001; Vivas et al., 2008) and DC (Chen & Pui, 1999; Hernandez-Sierra et al., 2003; Li & Chen, 2011; Qi et al., 2008), an AC electric field in the mixing zone does not reduce losses of nanoparticles, even under laminar flow conditions. The AC field seems to only affect the amount of ions reaching the charging region. This is probably explained by the fact that nanoparticles are susceptible to hydrodynamic forces from the ion wind or flow disturbances, which make losses to the walls unavoidable, irrespective of an additional electric field.

4. *Losses of particles*: The concentration of particles can decrease during the charging process due to diffusional losses (L_d), which refers to losses inside the charger with no electric field is applied (no ions). These losses are usually small for particles larger than 20 nm. The electrical losses (L_{el}) are additional losses of charged particles due to space charge effects. For small particles, losses are substantial because two competing effects influence the total: since the charging efficiency of ultrafine particles is lower than the rest of particles, the non-charged nanoparticles will suffer diffusional losses, while because of their higher mobility the electrical losses will increase.

To overcome the enumerated issues, the device operation characteristics are chosen as follows. The sheath gas for the present work was pure nitrogen (purified with Oxisorb, 99.9999% purity) because it is closest to air in its material properties (its breakdown voltage is only about 15% greater than air) and avoids the ozone generation. It has to be mentioned that N_2 is a non-electron attaching gas, efficient in slowing down electrons and thus is not able to form negative ions (Stano et al., 2009–2010). Therefore, only positive corona operation is shown here.

To prevent losses of aerosol particles due to the strong electric field when passing through the charger, the so-called indirect corona charger layout was applied (Li & Chen, 2011; Qi et al., 2007, 2008). The ionization and mixing zones are separated, therefore the reduction of the electric field strength in the charging region is expected to lead to a reduction of the charged particle losses inside the charger (Wiedensohler et al., 1994). It attenuates the erosion of the needle due to the use of clean nitrogen gas, thus it may remain stable for longer and avoids contamination of the electrode. Also, the introduction of a surrounding sheath air flow helps the charged particles to flow through the charger without excess precipitation on the charger walls (Intra & Tippayawong, 2011).

A tungsten needle was used as a discharge electrode, since this material has the highest melting point and the lowest vapor pressure of all metals, thereby is efficient for electron or ion emission. A constant electric field is formed by means of high voltage supplied to the electrode, since an alternate field does not offer any advantage and can lead to ion losses.

Generally, an ideal charger provides a balance between a high ion concentration and low particle losses, the capacity to work at various ambient conditions with no gas-to-particle conversion, low coagulation levels between charged particles and a predictable charge distribution for application to size selection of nanoparticles. The unipolar charger must lead to acceptable fractions of singly charged particles with minor fractions of multiply charged particles. Therefore, there is an interest to improve the unipolar corona discharge charger.

The corona charger proposed here is designed to be applied where radioactive neutralizers have been traditionally used. Ideally, it will have the possibility of reaching similar charge levels as radioactive neutralizers in order to easily replace them, and since it can be turned on and off there are no transportation restrictions, making it a good choice for field studies. It is experimentally confirmed that there is no particle generation inside the device, and it is designed for minimal waste of the needle and for a quick and an easy replacement without major changes in the charging efficiency.

The performance of the corona charger was assessed in experiments with monodisperse particles in the size range of 6–60 nm, aerosol flow rates between 0.5 and 1.5 lpm. Charging efficiencies and particle charge distributions were measured and compared to the ones obtained with a commercial radioactive bipolar charger.

2. Experimental setup

2.1. Design of the unipolar corona charger

Taking into account the objectives and drawbacks from prior instruments, the device is designed as a needle-based post-charging device, where ion generation and charging chambers are separated as can be seen in Fig. 1. This avoids contamination of the needle which results in a longer life time (Kwon et al., 2005; Qi et al., 2007). A tungsten needle is mounted on a micrometer-supported base, so that the distance to the output of the ionizing chamber can be modified and therefore the distance to the ground electrode can be precisely controlled during the experiment.
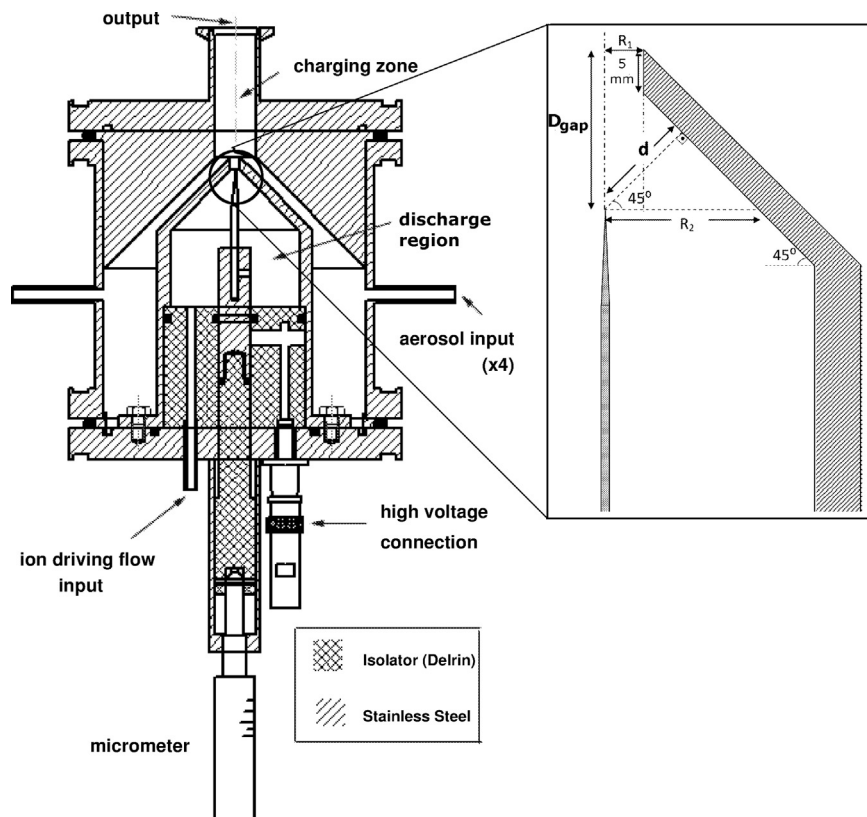
Fig. 1. Cross-section of the corona device. The inner part consists of the needle, the high voltage connection and the ion driving flow. The outer part, where particles come in, is separated from the inner up to the charging region, where the particle flow surrounds the ion flow.

The ion chamber is concentric to and surrounded by the particle flow, which as shown in a theoretical study (Alonso et al., 2009) is the best configuration for unipolar chargers. The advantage of cylindrical geometry is that distortion of electric field between electrodes is minimal due to the absence of corners and edges (Intra & Tippayawong, 2006).

Two different flows are applied for carrying ions, Q_i, and aerosol particles, Q_a. The particle-free flow that transports the ions out of the generation region prevents the penetration of particles into the corona discharging zone, while the 45° of inclination of the particle flow with respect to the ion flow helps the mixing of ions and particles.

As can be seen in Fig. 1, the distance between electrodes is different depending on the position of the needle. The corona discharge will be produced at the tip of the needle, and the field lines will be straight and perpendicular to the earthed surface. This means that for a position of the micrometer (D_{gap}) between 0 and 5 mm of distance from the needle tip to the outlet of the discharge region, the shorter distance to the earthed electrode will be the radius of the tube, since it has cylindrical geometry. For gaps from 5 mm onward, the shape of the earthed electrode is conical, and the perpendicular distance d to the surface can be calculated by trigonometry. For simplicity we will refer these distances from now on as the D_{gap} value, bearing in mind that the actual values of the distance between electrodes are the related d.

This configuration allows modification of a wide number of parameters such as the ion and aerosol driving flows, the length of the charging region by replacing or adding another tube, or the distance between the needle electrode to the earthed wall. All these features influence on the operation of the device, therefore determining the $N_i t$−product.

2.2. Experimental setup

To characterize the designed charger prototype, the experimental setup shown in Fig. 2 was used.

A distribution of SnO nanoparticles with an electrical mobility diameter below 60 nm was generated by the well-known evaporation–condensation technique (Scheibel & Porstendörfer, 1983). The carrier gas passing through the furnace is nitrogen at 1.5 lpm.

The aerosol passes first through a [85]Kr radioactive neutralizer, where the particles acquire a known charge distribution. A Nano-DMA (TSI-8085, Minneapolis, USA) with a fixed operating voltage classifies particles based on the electrical mobility. An aerosol with a monodisperse particle distribution passes then through a second [85]Kr neutralizer to neutralize the charged particles and then through an Electrostatic Precipitator (ESP) to remove the remaining charged particles. Only neutral particles with known size and concentration C_{in} are introduced in the test charger.
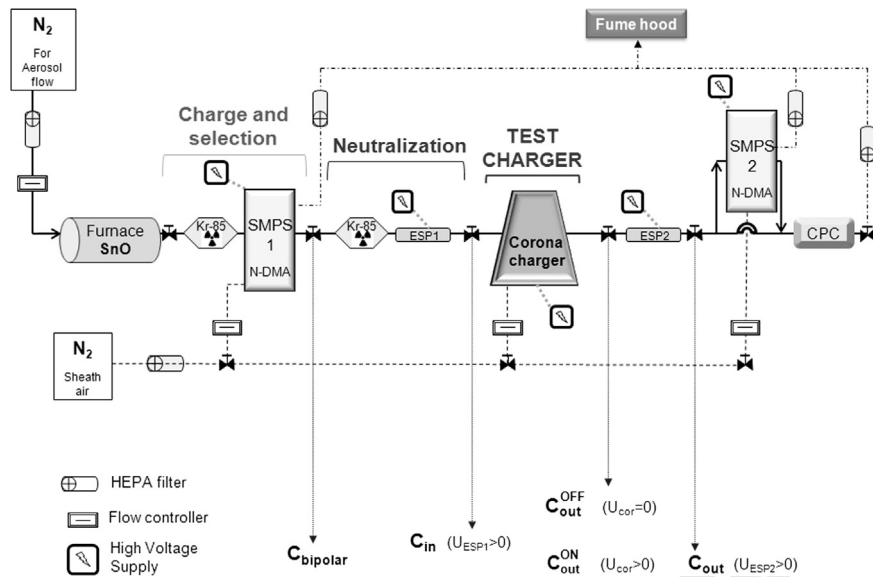
Fig. 2. Experimental setup for characterization of the corona charger.

At the exit of the prototype charger, monodisperse particles pass through a SMPS (TSI-3080 with Nano-DMA8085 and the ^{85}Kr neutralizer from the SMPS removed) in combination with a CPC (TSI-3775) to scan the size distribution, alternatively with the voltage on and off (C_{out}^{on} and C_{out}^{off} respectively) to measure the amount of charged particles and particle losses inside the device.

Since the proportion of charged particles cannot be directly measured, the charged particles are removed by means of a second precipitator after the corona charger. There, C_{out} is obtained, and the difference between C_{out}^{on} and C_{out} will give the concentration of charged particles.

3. Results

3.1. Corona current

Measurement of the ion current is done by means of an electrometer (model EL-5010, RAMEM, Madrid, Spain) which can measure in the femtoammeter range. The ion current at the outlet of the charging region was measured by means of a Faraday cup fabricated by RAMEM too. The collector was a stainless-steel tip connected with the electrometer device and isolated from the outer walls of the cage. The tip was fed with an applied bias voltage of 12 V to attract the ions to the collector.

A commercial DC high voltage power supply was used to maintain the voltages and currents in the ranges between 2.0–4.5 kV and 1–12 μA. The ions produced inside the charger are then led into the Faraday cup.

Firstly, the value of the corona onset voltage V_0 must be known, which has a strong dependence on the electrode tip radius and the inter-electrode distance (Henson, 1981). Despite the experimental and theoretical efforts made to predict V_0 accurately, its experimentally observed value varies under different conditions. It can be approximated by Peek's (1920) equation:

$$V_0 = m_v E_0 \delta \left(1 + \frac{0.308}{\sqrt{\delta r}}\right) r \ln\left(\frac{S}{r}\right) \tag{1}$$

where r is the radius of curvature of the tip of the needle, S is the distance between electrodes and 0.308 cm$^{1/2}$ is an empirical constant for cylindrical geometry. The relative air density factor δ is 1 at NTP, and the conductor roughness factor m_v is 1 for smooth cylindrical electrodes.

The disruptive voltage gradient is a value empirically calculated for the critical electric field that causes the medium (an insulating gas) to break down and become partially conductive. At NTP conditions, this electric field is around 15% larger for nitrogen than for air, i.e. $E_0(N_2) = 3.565 \times 10^6$ V/m.

The corona onset voltage can be determined experimentally as the point at which the current intersects the voltage axis V_c in Fig. 3. Measured and calculated corona onset voltages differ substantially, obtaining experimentally 1.95, 2.25 and 2.40 kV for electrode distances of 3, 7 and 10 mm, while calculated results are 2.03, 2.54 and 2.95 kV respectively.

The current experiences a first increase when the corona starts and then again rapidly increases when spark-over is reached. The corona discharge starts at lower voltages for a gap of 3 mm, while for the gap of 10 mm the range of applicable
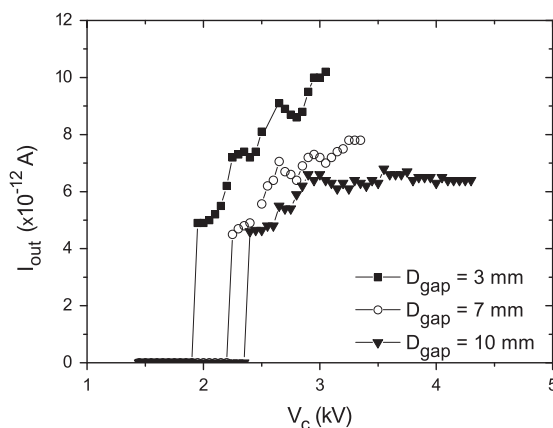
Fig. 3. Corona applied voltage versus output current at an ion dilution flow of 0.5 lpm and a sheath aerosol flow of 1.5 lpm.

corona voltages is greater, as can be seen in Fig. 3. But while the current of the 3 mm gap increases with applied voltage, in the case of 10 mm it tends to grow slowly, remaining approximately constant.

The reason is that the ion current depends exclusively on corona voltage only within a narrow interval (Intra & Tippayawong, 2010). At larger voltages it practically becomes constant, independent of the corona voltage, since a higher degree of ion loss is inevitable with a large number of ions, e.g. due to space charge effects.

In Fig. 4 the variation in corona is shown with the lower axis for a fixed corona applied current of 0.07 mA, and the variation of corona current for a fixed applied voltage of $V_c = 3.5$ kV with the upper axis. The measured output current is practically the same independent of the variation in applied voltage or current. Therefore in the following, unless the contrary is indicated, we will work by varying the voltage at fixed $I_c = 0.07$ mA for simplicity reasons.

3.2. Particle losses

The presence of particle losses can impose significant uncertainties in determining the true charging efficiency. They can be distinguished into two types of losses, the losses of neutral particles, mainly caused by diffusion,

$$L_d = 1 - F \cdot \frac{C_{out}^{off}}{C_{in}}, \qquad (2)$$

and losses of charged particles, related to the effect of electrostatic forces,

$$L_{el} = F \cdot \frac{C_{out}^{off} - C_{out}^{on}}{C_{in}}. \qquad (3)$$

The additional flow for driving ions Q_i makes it necessary to consider an auxiliary flow factor for aerosol dilution,

$$F = \frac{Q_i + Q_a}{Q_a} = \frac{Q_{out}}{Q_{in}}. \qquad (4)$$

There is some controversy on whether the definitions of losses and charging efficiency should be based on the particle number concentration itself (Hernandez-Sierra et al., 2003) or on the particle fluxes (i.e., particle concentration times the carrying flow rate) (Marquard et al., 2006b; Qi et al., 2007). For chargers with a supplementary gas flow like shown in Büscher et al. (1994), Chen & Pui (1999), and Medved et al. (2000), the aerosol concentration is diluted within the appliance. Due to different aerosol flow rates entering and leaving the charger, the concentration ratio cannot be obtained by measuring the particle number upstream and downstream the charger and shall therefore be based, for each particle size, on the total number of particles, not on the number concentration. That is, the measured number of particles is multiplied by the corresponding flow rate to obtain the particle flux in each stream. This is a factor to take into account for comparison with numerical results from other devices, even though dilution has no effect on the possibility of single particles to be charged.

Since the diffusional effect is significant only for particles smaller than approx. 20 nm, the diffusional losses are reduced with increasing diameter, having very strong losses (close the 50%) for $D_p < 10$ nm (Fig. 5).

However, when the charger is switched on there are additional electrostatic losses. Electrical losses for the needle position of 3 mm are much greater (above 20% for the smallest diameters) than for the gap of 10 mm, which barely reach 2%. This effect is related to the ion concentration, since with a lower needle position the electric field is more shielded from the charging region, so that the particles are more likely to be lost by electrostatic effects.

When the corona is switched on, the ion concentration is 'diluted' with the ratio of the ionizer flow rate to the total flow rate. Thus, the $N_i t$−product can be changed by varying this ratio, since a small Q_i in comparison to the Q_a leads to a strong
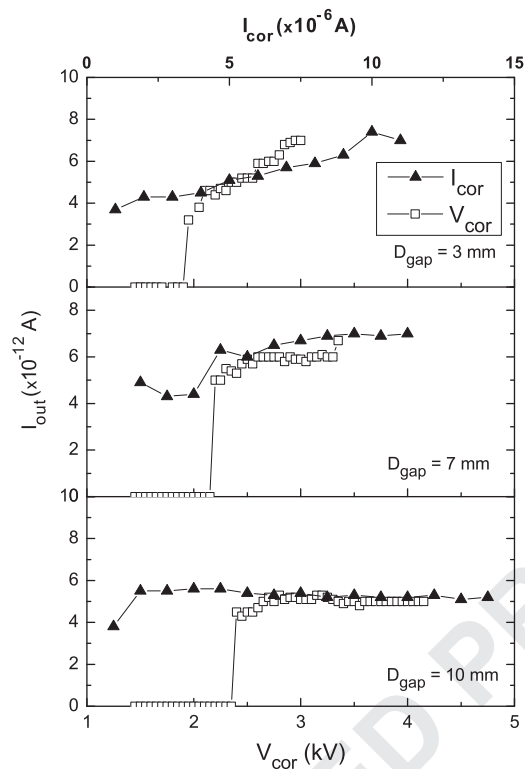
Fig. 4. Measured output current for variation of the applied current (upper axis) at a fixed corona voltage of $V_c = 3.5$ kV and the applied voltage (lower axis) at a constant corona current of $I_c = 7$ μA.
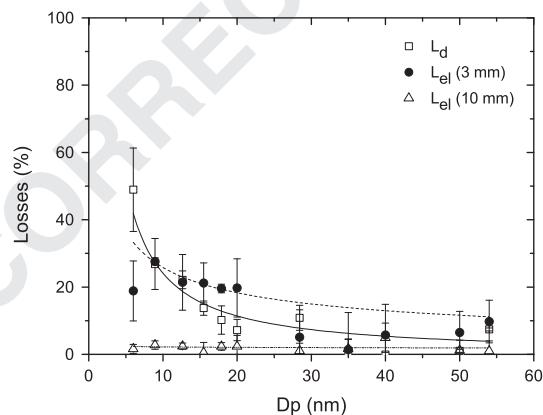

Fig. 5. Losses of charged and neutral particles for several particle diameters at different distances between electrodes.

decrease in the ion concentration and thereby of the $N_i t$−product, on the other hand a high Q_i would lead to a high ion concentration but also a strong decrease in effective particle concentration. Therefore, an optimal flow balance has to be found.

Selecting particles having a diameter of 15 nm and fixing Q_a at 1.5 lpm, three different ion flow rates were tested and losses of neutral and charged particles determined. In Table 1 it is shown for neutral particles that the larger the ion flow Q_i, the higher the particle losses. This cannot be explained by diffusion losses, as the reduced time when increasing the ion flow rate should lead to smaller diffusion losses. However, the turbulence level might increase due to the inclined mixing arrangement, which explains the increasing losses. The same happens when particles are charged for the case of 10 mm gap. On the contrary, for the 3 mm gap, losses of charged particles slightly decrease with increasing ion flow. This is probably due to the shorter residence time which reduces the loss of charged particles, where the loss mechanism is probably due to the space charge effect of the ions entering the charging region.

Table 1

Losses for neutral L_d and charged L_{el} particles of 1.5 nm at different corona operating voltages for an aerosol flow rate Q_a of 1.5 lpm and three different ion dilution flow rates. Two different distances from the electrode needle to the output were tested, 3 mm and 10 mm.

	V_c (kV)	Q_i (lpm)→	D_{gap} = 3 mm			D_{gap} = 10 mm		
			0.5	1.0	1.5	0.5	1.0	1.5
	2.0		28.5	23.5	16.5	–	–	–
	2.5		43.5	35.0	30.4	9.8	22.1	34.5
L_{el} (%)	3.0		–	–	–	10.2	21.9	35.7
	3.5		–	–	–	11.0	22.4	35.7
	4.0		–	–	–	11.6	21.1	35.7
L_d (%)			1.0	10.6	14.5	1.0	10.6	14.5

Likewise, an increase in voltage will increase the ion concentration and therefore the electrical losses due to a stronger space charge effect, as is shown for 3 mm gap. But in the case of 10 mm gap, losses are almost constant with the increase in corona voltage, from which can be inferred that the space charge effect has a limited impact at this electrode distances.

It is seen that a higher total flow increases the losses, but when it is fixed, the ratio of ion to aerosol flow also has an effect on the particle deposition in the charger. Losses can be expressed also in the form of the penetration of the particles through the setup. An accurate calculation of the penetration has to take into account the total loss of charged particles $L_T = L_{el} + L_d$:

$$P_n = 1 - L_T = F \cdot \frac{C_{out}^{on}}{C_{in}} \qquad (5)$$

In Fig. 6 the penetration is shown as a function of the ratio of ion to aerosol flow for the incoming charged particles. It can be seen that a ratio greater than 1 leads to a very low penetration of charged particles through the charger, and shall be avoided. The increasing space charge effect of the incoming ions at higher Q_i/Q_a ratios drives the particles towards the outer walls, leading to lower penetration. From the graph, an acceptable ratio of the flows is 0.33, which corresponds to $Q_i = 0.5$ lpm and $Q_a = 1.5$ lpm and will be used in the following.

3.3. Charging efficiencies

For the complete characterization of a charger it is necessary to measure particle loss, charging efficiency and charge distribution. The charging efficiency is the most important performance parameter for aerosol chargers, since it describes the possibility of an individual particle to acquire charges during the process.

Depending on the success of the particle to pass through the charger, this efficiency can be classified as intrinsic charging efficiency, ξ_{int}, when only the rate of particles being charged is important, or extrinsic charging efficiency, ξ_{ext}, when also the success to properly reach the outlet of the device is taken into account. Discrepancy between intrinsic and extrinsic charging efficiencies is attributed to the charged particle losses inside the charger (Qi et al., 2007).

The comparison of efficiencies is based exclusively on external measurements; knowledge of the internal physical charging conditions such as $N_i t$−product or electrical field is not required (Marquard et al., 2006b).

The intrinsic efficiency contains information about the 'true' charging probability of the particles, the total of the charged particles leaving the charger compared with the neutralized particles going in. Additional assumptions for its experimental determination are needed by considering the particles that were lost as a part of the totals:

$$\xi_{int} = \frac{C_{out}^{q} + L_{el}}{C_{in} - L_d} = 1 - \frac{C_{out}^{0}}{C_{out}^{off}} \qquad (6)$$

On the other side, the extrinsic charging efficiency is the 'final' efficiency, the efficiency at which the corona charger will operate. It can be determined experimentally without additional assumptions, considering the quantity of charged particles exiting versus the total entering the charger:

$$\xi_{ext} = F \cdot \frac{C_{out}^{on} - C_{out}^{0}}{C_{in}} \qquad (7)$$

However, its definition also contains implicit information of losses and one cannot distinguish the contribution of these losses to the extrinsic efficiency unless all particles are considered to be charged (Marquard et al., 2006b).

The charging efficiency is expected to rise with particle diameter and with ion concentration, whereas the intrinsic efficiency should be higher for the gap of 3 mm since more ions are generated.

The balance of flows has a manifest impact on efficiencies, as it had on losses. When the total flow increases, residence time is shortened and the ion concentration decreases due to dilution. With a constant total flow rate, a higher dilution flow increases both the intrinsic and extrinsic charging efficiencies (Fig. 7) because of the higher number of ions that is supplied to the aerosol, apparently compensating the smaller residence time and the increase of electrical losses. This effect is more evident for the 10 mm gap, since the ion concentration is lower and more ion flow drags more ions, reducing losses.
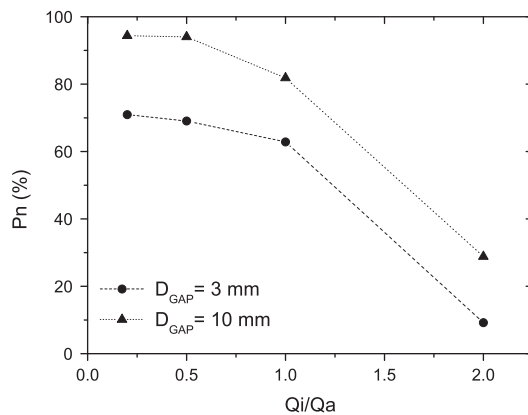
Fig. 6. Measured penetration for charged particles of 50 nm at different flow ratios for a fixed total flow rate of 2 lpm and an applied corona voltage of 3.5 kV.
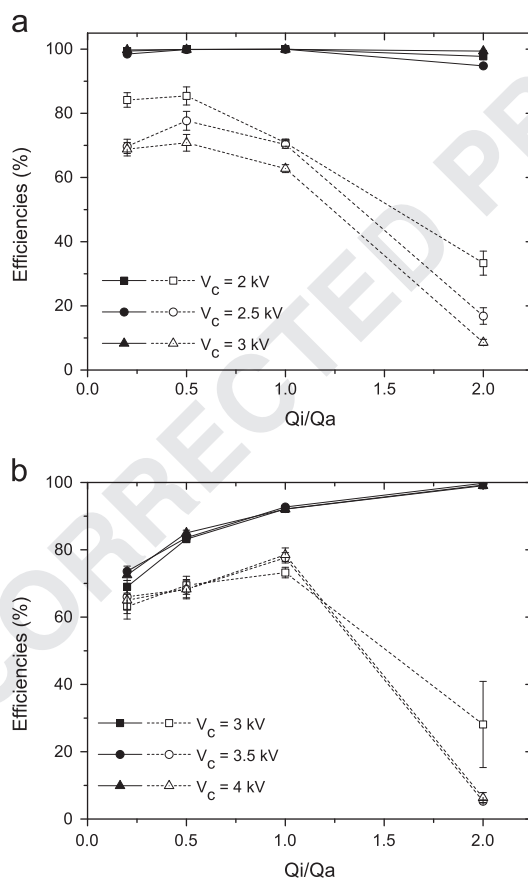

Fig. 7. Intrinsic (solid symbols) and extrinsic (empty symbols) charging efficiencies of 50 nm particles for different flow ratios at a fixed total flow rate of 2.0 lpm. (a) refers to an electrode gap of 3 mm and (b) to 10 mm. Three different voltages are used for each measurement.

But when the ion flow is larger than the aerosol flow, extrinsic charging efficiency decreases drastically since most of ions are lost by the large space charge effect, which is supported by the fact that the intrinsic charging efficiency is unaffected by the flow ratios.

The operating voltage V_c does not influence the intrinsic charging efficiency. However, for a gap of 3 mm, the higher the voltage the lower the extrinsic efficiency, which is not the case for 10 mm. The reason can be found in Fig. 4, which shows an increase in output current for 3 mm but not for 10 mm gap distance.

Figure 8 shows that efficiencies increase with the particle diameter since larger particles tend to acquire easily more than one charge per particle. Also the effect of the inter-electrode distance on the charging by sizes is compared, determining that
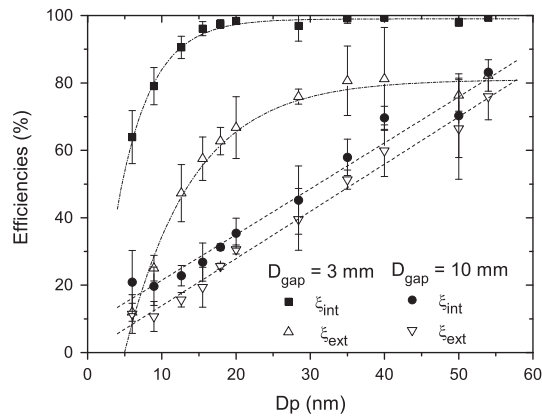
Fig. 8. Variation of intrinsic (solid symbols) and extrinsic (empty symbols) charging efficiencies with particle diameters for gaps of 3 mm and 10 mm.
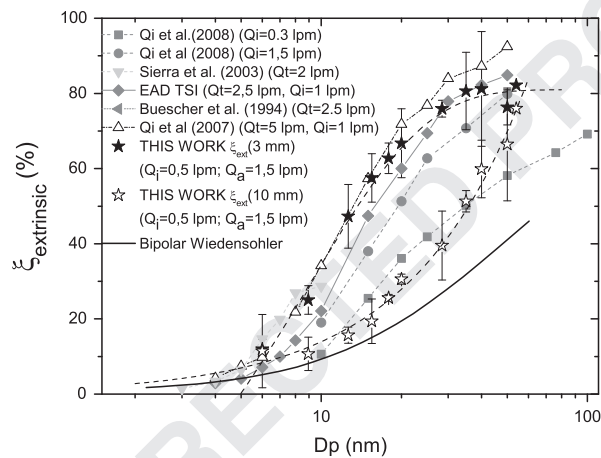

Fig. 9. Extrinsic efficiencies for different particle sizes and gap distances compared with values from other devices presented in the literature.

for the 3 mm gap, the intrinsic efficiency reaches practically 100% from 18 nm particles. Previously the effect of diffusional losses was found to be strong for small particles (see Fig. 5) and the charging efficiency for diameters of 6 nm is around 65%. When the gap increases up to 10 mm, therefore diminishing the ion concentration, the intrinsic efficiency is much smaller, e.g. 50% for the particles with 40 nm in diameter.

In the case of extrinsic efficiencies, at diameters below 15 nm the combination of electrical and diffusional losses is strong enough to decrease the real charging efficiency below 20% with the 3 mm gap. But following values are as high as 80% for 35 nm particles. However, for the 10 mm gap, the difference between intrinsic and extrinsic efficiencies is around 15%, even less as the particle size grows, which means that the 'true' and the 'final' efficiency (i.e. intrinsic and extrinsic respectively) are quite close due to the smaller losses.

In Fig. 9, the extrinsic charging efficiency of the charger is compared as a function of particle diameter with collected data from other corona-based aerosol chargers. Results of the extrinsic efficiencies of Qi et al. (2007) are included, along with data from Büscher et al. (1994), Hernandez-Sierra et al. (2003) and Qi et al. (2008), and also the charging efficiency in the case of bipolar charging (TSI Inc., 2006; Wiedensohler, 1988) is plotted for reference.

The charging efficiency used in this study refers to the charged particles flux, which is different from the definition presented in other works (the fraction of charged particles among all the particles exiting from the charger). For this reason, the selected data for reference are from chargers that consider dilution, except that of Hernandez-Sierra et al. (2003), in which there was no dilution of the aerosol stream.

It can be seen that a wide spectrum of charging efficiencies is covered by the charger presented in this work when moving from a 3 to a 10 mm electrode gap. For particles as large as 35 nm and a gap of 3 mm, efficiencies of around 85% are reached, comparable with other highly efficient chargers, while with a 10 mm gap, lower efficiencies are attained, close to that of radioactive chargers for particles below 20 nm. Changing the position of needle electrode can adjust the $N_i t$−product and therefore the charging levels as the user desires.

3.4. Charge distribution

Since the particle size distribution usually based on measurement of the electrical mobility, a known and predictable charge distribution must be imposed on the aerosol. For this purpose, the mobility distribution of the charged particles is measured with the help of a second DMA after the test charger, as can be seen in Fig. 2.

The different peaks in Fig. 10 (for a particle diameter of 35 nm as an example) correspond to the different numbers of charges on the particles. The relative area under each peak gives the fraction of charged particles carrying a certain number of elementary charges. To obtain absolute magnitudes, the number fraction is normalized so that the total area under the curves is one. For each particle diameter, this fraction of area is multiplied by the corresponding extrinsic charging efficiency, returning the fraction of charged particles.

The y-axis shows the number concentration normalized in such a way that the total area under the curve is 1. The whole scanning range of the Nano-DMA is covered, but due to the shape of the original distribution, the number of particles in the tails is much lower than close to the central diameter. This can cause a voltage shift, as it was explained by Alonso & Kousaka (1996). They showed that when particles classified by a DMA are passed through an identical second DMA operating with the same flow rates, the mean classification voltage for the second unit is usually different from the fixed voltage applied to the first one, and the shifts are larger for particles in the tails, where concentration is lower than the mean.

In our case, the voltage shift is around 1 nm, as can be seen in the different plots of Fig. 10, reaching 1.5 nm in the worst cases where concentration was relatively low. Considering the accuracy of the voltage supply from the device, which as provided by manufacturer's is ± 1 V for applied voltages under 500 V, ± 6 V for voltages below 5 kV and ± 2 V for voltages up to ± 10 kV, and the uncertainty from the gas flow controllers, the error in the diameter is smaller than 1% (mostly between 0.2% and 0.8%), and is within the accuracy of the SMPS.

A software was created to fit the curves and calculate the areas and mean diameters of each peak. The best fit calculation is based on Differential Evolution (DE) (Strorn & Price, 1997), a method that optimizes a problem by iteratively trying to improve a candidate solution with regard to a given measure of quality. DE is based on the following steps: a fixed number of vectors are randomly initialized, then evolved over time to locate the minima of the objective function. At each iteration (generation), new vectors are generated by the combination of vectors randomly chosen from the current population (mutation). The out-coming vectors are then mixed with a predetermined target vector (recombination) and produces the trial vector. Finally, the trial vector is accepted for the next generation if and only if it yields a reduction in the value of the
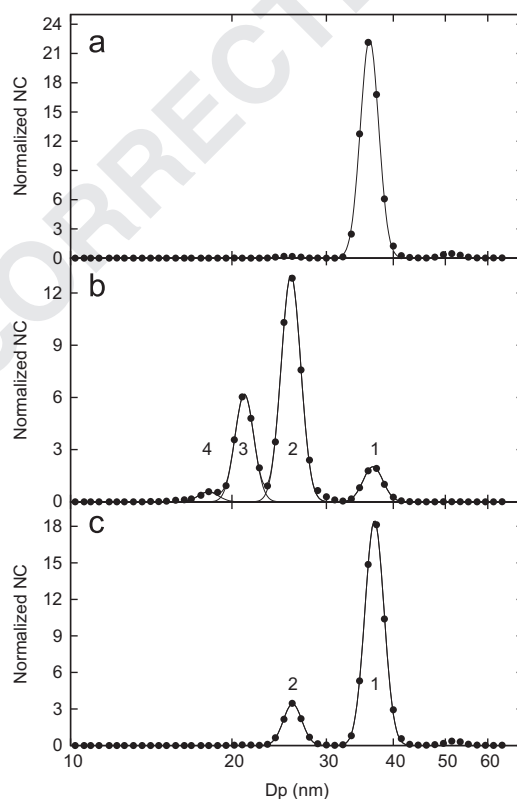

Fig. 10. Normalized number concentration (NC) before and after the test charger for two gap distances at $Q_a = 1.5$ lpm and $Q_i = 0.5$ lpm. (a) is the distribution before corona, from the bipolar charging for reference, (b) and (c) are for corona charging for an applied voltage of 3.5 kV and electrodes gap of 3 mm and 10 mm respectively.

objective function (selection). DE can be used on optimization problems that are noisy, non-differentiable, nonlinear or change over time, since it does not require the problem to be differentiable.

In our case, we fit the sum of Gaussians by DE taking as reference the quadratic error, and from the results calculates the area under each curve and the corresponding geometric mean diameter, as well as the standard deviation of each peak. To help the algorithm in the search for peaks, the number of log-normals and the mobility equivalent diameters were provided, since sometimes were too close each other and they could not be distinguished by the software itself. Peaks with an area of less than 1% were discarded.

Peaks appearing at the right of the nominal diameter are produced by particles which acquired a double charge in the [85]Kr charger at the DMA-1 and were classified because they have the same electrical mobility as the singly charged. They are usually unnoticed in the bipolar plot since they are classified within the peak of the selected voltage. Anyway, the fraction of these particles is negligible in comparison with that of the main aerosol.

The experimentally found charge distributions are shown in Fig. 11 for particles with diameters between 6 and 60 nm for two different electrode gaps and an optimum corona voltage of 3.5 kV, which maximizes the extrinsic efficiency. It can be seen that the number of charges per particle can be adjusted by moving the electrodes. When the needle is at the gap of 3 mm, particles acquire up to 6 charges, having a wide range of doubly and triply charged particles, while further away, the fraction of doubly charged particles is below 10% for diameters under 35 nm (Fig. 11(b)). This means that for smaller electrode gaps, the effective $N_i t$−product is higher than for larger ones, which can easily be explained by a larger number of ions moving from the corona region into the charging zone. This effect can be very clearly seen in the charging level, however when looking at the measured output current (Fig. 4), the differences between the output current for the 3 and 10 mm electrode gap are relatively small. Measuring the effective output current as a means to gain information on the effective $N_i t$−product is therefore not a good strategy.

The low amount of charges per particle facilitates the electrical mobility analysis for aerosol sizing, and a comparison with a bipolar charger in Fig. 11(b) (data from SMPS-3080 from TSI, with a [85]Kr charger (TSI Inc., 2006; Wiedensohler, 1988) shows that for particles below 20 nm could be possible a substitution of the radioactive chargers by this device. Notice that these results were obtained for certain characteristics, such as flow rates and voltages (therefore $N_i t$), and changing these can lead to results even closer to the bipolar distribution.
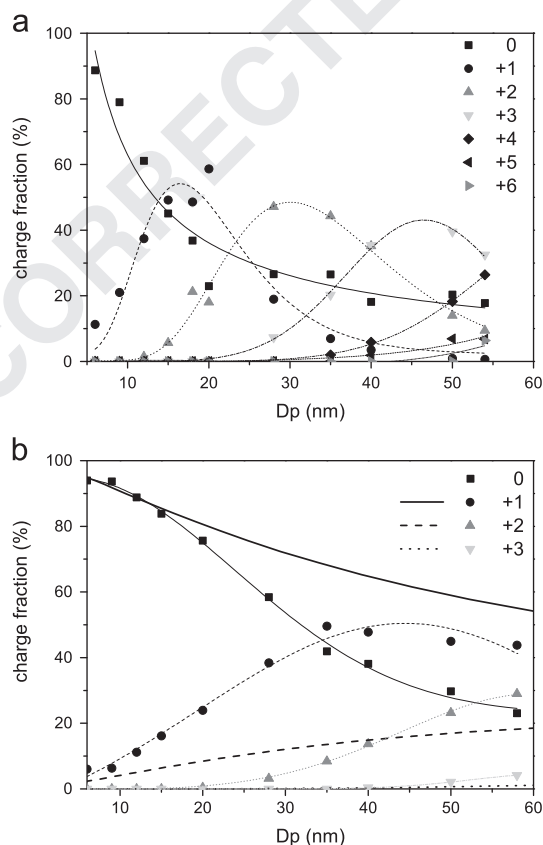

Fig. 11. Charge distribution as a function of diameter for electrode gaps of (a) 3 mm and (b) 10 mm for flow rates of $Q_a = 1.5$ lpm and $Q_i = 0.5$ lpm and the applied voltage of 3.5 kV. In (b) the bipolar distribution from Wiedensohler (1988) is shown as thick lines for comparison.

The results show that having an electrode gap distance which can be easily varied is a very effective method to vary the effective $N_i t$−product. In Fig. 4, it can be seen that changing the corona current has only a limited effect on the measured output current. Therefore, it can be concluded that changing the electrode gap distance is a better strategy to vary the $N_i t$−product than changing electrical characteristics such as corona current.

4. Conclusions

A new indirect corona device with cylindrical geometry was designed and tested. It is a flexible design in which many of the features can be modified for a better control of the charging process, as well as the reproducibility of the results. It has a sheath flow to drive the ions towards the charging zone, avoiding the direct contact of aerosol and corona needle.

The developed corona charger is able to vary the $N_i t$−product over a wide range, for smaller values which lead to charging levels close to the bipolar charge equilibrium, as well as high values which lead to high charging levels which are relevant for electrostatic particle deposition or particle detection devices which become more sensitive when the charging level increases. Thus, it can perform in a similar way as radioactive neutralizers, as well as obtain high efficiencies as the previous unipolar devices. This could be significant in substitution of such radioactive devices by a unipolar source which has similar characteristics but is exempt of the restrictions due to the radioactivity. It has a wide range of charging efficiencies for the nanoparticle range, adjustable by controlling the amount of ion concentration by the position of the needle electrode. This method of adjusting the $N_i t$−product seems to result in a broader range of charging levels than by adjusting electrical characteristics such as corona current.

Though the particle losses are relatively high, they are comparable to other devices shown in the literature and can probably be reduced by optimizing further the flows or the corona voltage. It is remarkable also that an ion flow equal or greater than the aerosol flow leads to high losses, so a more detailed study of this effect might lead to further optimization of the charging conditions.

References

Alguacil, F., & Alonso, M. (2006). Multiple charging of ultrafine particles in a corona charger. *Journal of Aerosol Science*, *37*(7), 875–884.

Alonso, M., Alguacil, F.J., & Borra, J.P. (2009). A numerical study of the influence of ion–aerosol mixing on unipolar charging in a laminar flow tube. *Journal of Aerosol Science*, *40*(8), 693–706.

Alonso, M., & Kousaka, Y. (1996). Mobility shift in the differential mobility analyzer due to Brownian diffusion and space-charge effects. *Journal of Aerosol Science*, *27*(8), 1201–1225.

Alonso, M., Martin, M.I., & Alguacil, F.J. (2006). The measurement of charging efficiencies and losses of aerosol nanoparticles in a corona charger. *Journal of Electrostatics*, *64*(3–4), 203–214.

Biskos, G., Reavell, K., & Collings, N. (2005a). Electrostatic characterisation of corona–wire aerosol chargers. *Journal of Electrostatics*, *63*(1), 69–82.

Biskos, G., Reavell, K., & Collings, N. (2005b). Unipolar diffusion charging of aerosol particles in the transition regime. *Journal of Aerosol Science*, *36*(2), 247–265.

Büscher, P., Schmidt-Ott, A., & Wiedensohler, A. (1994). Performance of a unipolar "square wave" diffusion charger with variable nt-product. *Journal of Aerosol Science*, *25*(4), 651–663.

Chen, D.R., & Pui, D.Y.H. (1999). A high efficiency, high throughput unipolar aerosol charger for nanoparticles. *Journal of Nanoparticle Research*, *1*(1), 115–126.

Henson, B.L. (1981). A space-charge region model for microscopic steady coronas from points. *Journal of Applied Physics*, *52*(2), 709–715.

Hernandez-Sierra, F.J., Alguacil, A., & Alonso, M. (2003). Unipolar charging of nanometer aerosol particles in a corona ionizer. *Journal of Aerosol Science*, *34*(6), 733–745.

Hewitt, G.W. (1957). The charging of small particles for electrostatic precipitation. *AIEE Transactions*, *76*, 300–306.

Intra, P., & Tippayawong, N. (2006). Aerosol size distribution measurement using multi-channel electrical mobility sensor. *Aerosol and Air Quality Research*, *21*(4), 329–340.

Intra, P., & Tippayawong, N. (2010). Effect of needle cone angle and air flow rate on electrostatic discharge characteristics of a corona-needle ionizer. *Journal of Electrostatics*, *68*(3), 254–260.

Intra, P., & Tippayawong, N. (2011). An overview of unipolar charger developments for nanoparticle charging. *Journal of Aerosol Research*, *11*, 187–209.

Kim, D.S., Kim, Y.M., Kwon, Y.T., & Park, K. (2010). Evaluation of a soft x-ray unipolar charger for charging nanoparticles. *Journal of Nanoparticle Research*, *13*, 579–585.

Kleefsman, W.A., & Van Gulijk, C. (2008). Robust method to compare aerosol chargers. *Journal of Aerosol Science*, *39*(1), 1–9.

Kruis, F.E., & Fissan, H. (2001). Nanoparticle charging in a twin Hewitt charger. *Journal of Nanoparticle Research*, *3*(1), 39–50.

Kwon, S., Fujimoto, T., Kuga, Y., Sakurai, H., & Seto, T. (2005). Characteristics of aerosol charge distribution by surface-discharge microplasma aerosol charger (SMAC). *Aerosol Science & Technology*, *39*(10), 987–1001.

Kwon, S., Sakurai, H., Seto, T., & Kim, Y. (2006). Charge neutralization of submicron aerosols using surface-discharge microplasma. *Journal of Aerosol Science*, *37*(4), 483–499.

Li, L., & Chen, D.R. (2011). Performance study of a DC-corona-based particle charger for charge conditioning. *Journal of Aerosol Science*, *42*(2), 87–99.

Liu, B.Y.H., & Pui, D.Y.H. (1975). On the performance of the electrical aerosol analyzer. *Journal of Aerosol Science*, *6*(3–4), 249–264.

Marquard, A., Meyer, J., & Kasper, G. (2006a). Characterization of unipolar electrical aerosol chargers—Part II: Application of comparison criteria to various types of nanoaerosol charging devices. *Journal of Aerosol Science*, *37*(9), 1069–1080.

Marquard, A., Meyer, J., & Kasper, G. (2006b). Characterization of unipolar electrical aerosol chargers—Part I: A review of charger performance criteria. *Journal of Aerosol Science*, *37*(9), 1052–1068.

Medved, A., Dorman, F., Kaufman, S., & Pocher, S. (2000). A new corona-based charger for aerosol particles. *Journal of Aerosol Science*, *31*, 616–617.

Peek, F.W. (1920). *Dielectric phenomena in high voltage engineering*. McGraw-Hill Book Company, inc.: .

Qi, C., Chen, D.R., & Greenberg, P. (2008). Performance study of a unipolar aerosol mini-charger for a personal nanoparticle sizer. *Journal of Aerosol Science*, *39*(5), 450–459.

Qi, C., Chen, D.R., & Pui, D.Y.H. (2007). Experimental study of a new corona-based unipolar aerosol charger. *Journal of Aerosol Science*, *38*(7), 775–792.

Scheibel, H.G., & Porstendörfer, J. (1983). Generation of monodisperse Ag- and NaCl-aerosols with particle diameters between 2 and 300 nm. *Journal of Aerosol Science*, *14*, 113–126.

Stano, M., Sabo, M., Kučera, M., Matejčík, S., Han, H.Y., Wang, H.M., & Chu, Y.N. (2009–2010). Ion mobility spectrometry study of negative corona discharge in nitrogen–oxygen mixtures in nitrogen drift gas. *Acta Physica Universitatis Comenianae*, *L–LI*(1 & 2), 77–83.

Strorn, S., & Price, K. (1997). Differential evolution—A simple and efficient heuristic for global optimization over continuous spaces. *Journal of Global Optimization*, *11*, 341–359.

TSI Inc. (2006). *Operation and service manual for electrostatic classifiers*, series 3080, revision g.

Vivas, M., Hontañón, E., & Schmidt-Ott, A. (2008). Reducing multiple charging of submicron aerosols in a corona diffusion charger. *Aerosol Science and Technology*, *42*(2), 97–109.

Wiedensohler, A. (1988). An approximation of the bipolar charge distribution for particles in the submicron size range. *Journal of Aerosol Science*, *19*(3), 387–389.

Wiedensohler, A., Büscher, P., Hansson, H., Martinsson, B., Stratmann, F., Ferron, G., & Busch, B. (1994). A novel unipolar charger for ultrafine aerosol particles with minimal particle losses. *Journal of Aerosol Science*, *25*(4), 639–649.